

# Metadata of the chapter that will be visualized in SpringerLink

Book Title	Cavitation Instabilities and Rotordynamic Effects in Turbopumps and Hydroturbines	
Series Title		
Chapter Title	From Cavitating to Boiling Flows	
Copyright Year	2017	
Copyright HolderName	CISM International Centre for Mechanical Sciences	
Corresponding Author	Family Name	<b>Saurel</b>
	Particle	
	Given Name	<b>Richard</b>
	Prefix	
	Suffix	
	Division	
	Organization	University Institute of France
	Address	Paris, France
	Division	
	Organization	Aix-Marseille University, CNRS M2P2
	Address	Marseille, France
	Division	
	Organization	RS2N
	Address	Marseille, France
	Email	richard.saurel@univ-amu.fr
Author	Family Name	<b>Métayer</b>
	Particle	<b>Le</b>
	Given Name	<b>Olivier</b>
	Prefix	
	Suffix	
	Division	
	Organization	Aix-Marseille University, CNRS IUSTI
	Address	Marseille, France
	Email	
Author	Family Name	<b>Boivin</b>
	Particle	
	Given Name	<b>Pierre</b>
	Prefix	
	Suffix	
	Division	
	Organization	Aix-Marseille University, CNRS M2P2
	Address	Marseille, France
	Email	
Abstract	A flow model is derived for the numerical simulation of interfacial flows with phase transition. The model arises from the classical multi-component Euler equations, but is associated to a non-classical	

thermodynamic closure: each phase is compressible and evolves in its own subvolume, with phases sharing common pressure, velocity and temperature, leading to non-trivial thermodynamic relations for the mixture. Phase transition is made possible through the introduction of Gibbs free energy relaxation terms in the equations. Capillary effects and heat conduction—essential in boiling flows—are introduced as well. The resulting multi-phase flow model is hyperbolic, valid for arbitrary density jumps at interfaces as well as arbitrary flow speeds. Its capabilities are illustrated successively through examples of nozzle induced cavitation and heated wall induced boiling.

---

# From Cavitating to Boiling Flows

Richard Saurel, Olivier Le Métayer and Pierre Boivin

**Abstract** A flow model is derived for the numerical simulation of interfacial flows with phase transition. The model arises from the classical multi-component Euler equations, but is associated to a non-classical thermodynamic closure: each phase is compressible and evolves in its own subvolume, with phases sharing common pressure, velocity and temperature, leading to non-trivial thermodynamic relations for the mixture. Phase transition is made possible through the introduction of Gibbs free energy relaxation terms in the equations. Capillary effects and heat conduction—essential in boiling flows—are introduced as well. The resulting multi-phase flow model is hyperbolic, valid for arbitrary density jumps at interfaces as well as arbitrary flow speeds. Its capabilities are illustrated successively through examples of nozzle induced cavitation and heated wall induced boiling.

## 1 Introduction

Cavitating, boiling and evaporating are three phenomena that involve phase transition in multi-phase flows. They appear in countless engineering applications: steam generators, marine propellers, liquid fuel combustion, etc. Yet, modelling these phenomena remains an unsettled problem.

Cavitation in a liquid is a phase change phenomenon created by a pressure drop driven by (fast) acoustic waves, generating—as its name suggests—large cavities. When pressure becomes lower than the saturation one at the local temperature,

---

R. Saurel (✉)  
University Institute of France, Paris, France  
e-mail: richard.saurel@univ-amu.fr

O. Le Métayer  
Aix-Marseille University, CNRS IUSTI, Marseille, France

R. Saurel · P. Boivin  
Aix-Marseille University, CNRS M2P2, Marseille, France

R. Saurel  
RS2N, Marseille, France

© CISM International Centre for Mechanical Sciences 2017  
L. d'Agostino and M.V. Salvetti (eds.), *Cavitation Instabilities and Rotordynamic Effects in Turbopumps and Hydroturbines*, CISM International Centre for Mechanical Sciences 575, DOI 10.1007/978-3-319-49719-8\_10

1

20 phase change appears as the liquid internal energy or temperature is greater than  
21 the saturated one: the liquid is overheated. Indeed, during a pressure drop, the liq-  
22 uid temperature varies weakly and at low pressure it becomes hot compared to the  
23 saturation temperature, this one being strongly dependant of pressure.

24 Boiling is yet another phase transition phenomenon created by heat deposition in  
25 a liquid, most times by heat conduction from a hot wall. The heating increases the  
26 liquid temperature and when it becomes greater than the saturation temperature at  
27 local pressure (most times uniform in the domain) phase change appears. Therefore,  
28 unlike cavitation, this process is governed by (slow) heat conduction.

29 In both instances, the liquid is overheated due to a departure from the saturation  
30 conditions, whether it comes from a pressure drop (cavitation) or from a tempera-  
31 ture rise (boiling). Consequently, phase change occurs, provided that some impurities  
32 (nucleation sites) are present. In industrial and natural fluids impurities are always  
33 present in large enough concentrations (solute gases, trapped bubbles in wall rough-  
34 ness etc.). Cavitation is oftentimes assumed to be isothermal, with severe pressure  
35 gradients, whereas boiling and evaporation are roughly isobaric, with important tem-  
36 perature gradients (Sinibaldi et al. 2006; d'Agostino and Salvetti 2008; Goncalves  
37 and Patella 2009). Although they have different characteristic times, as pressure gra-  
38 dients are associated to acoustic waves (fast), and temperature gradients to heat con-  
39 duction (slow), cavitation, boiling and evaporation are driven by phase transition and  
40 may therefore be modelled by the same approach.

41 However, in the literature, cavitation and boiling flows are considered through  
42 very different approaches. Most cavitation models consider liquid and two-phase  
43 mixture evolving at uniform temperature (Coutier-Delgosha et al. 2003; Barre et al.  
44 2009). In these formulations the flow model is barotropic and the energy conserva-  
45 tion principle as well as the second law of thermodynamics are omitted. In these  
46 models, the EOS is built to mimic some behaviour of two-phase mixtures, such as  
47 the mixture sound speed that evolves non-monotonically with respect to the volume  
48 fraction.

49 Boiling flows are considered by different approaches, most of them being based  
50 on Cahn and Hilliard (1958) approach of capillary fluids. Here the energy equation is  
51 considered as the importance of energetic effects are obvious. Contrarily to cavitation  
52 models, sound propagation is wrongly considered, as the square sound speed may  
53 become negative in the phase change domain (Menikoff and Plohr 1989). Indeed,  
54 the EOS is of cubic-type (van der Waals for example), with undefined sound speed  
55 in specific thermodynamic domain. Many other restrictions appear with the Cahn-  
56 Hilliard second gradient theory, such as for example the need to enlarge interfaces to  
57 make possible practical computations (Jamet et al. 2001). Fundamental issues also  
58 arise, such as shock wave existence in these media. The two most popular approaches  
59 for cavitating and boiling flows have consequently obvious limitations and restric-  
60 tions.

61 In the present work a unified approach is provided and its ability to model  
62 and compute cavitating and boiling flows is shown with computational examples.  
Most of the scientific material results from former investigations by Saurel (2008),

63 Le Martelot et al. (2013, 2014). The flow model is a hyperbolic system of partial  
 64 differential equations with Gibbs free energy relaxation. The thermodynamic clo-  
 65 sure is built without ambiguity and results in a mixture EOS valid in pure liquid,  
 66 pure vapour and two-phase mixture. The presence of non-condensable phase may be  
 67 considered as well. The sound speed is defined in all space of variables. Nonlinear  
 68 waves, such as shocks have a clear definition too. Last, the formulation is valid for  
 69 any flow speed and any fluid density ratio at interfaces.

## 70 2 Basic Flow Model Specification

71 The flow model has to deal with:

- 72 (a) Liquid and gas compressibility: liquid compressibility consideration is manda-  
 73 tory in cavitating flows and gas compressibility must be addressed in most situ-  
 74 ations of flows with phase change.
- 75 (b) Pure liquid and pure gas dynamics as well as interfaces motions, these ones  
 76 separating pure phases and those of two-phase mixtures.
- 77 (c) Mass exchange in mixtures and at interfaces, for both evaporation and conden-  
 78 sation.
- 79 (d) Heat conduction, important in boiling flows.
- 80 (e) Capillary effects, important in boiling flows as well.

81 Obviously the flow model has to be in agreement with the basic principles of physics  
 82 such as mass, momentum and energy conservation, second law of thermodynam-  
 83 ics, frame invariance and thermodynamic consistency (convexity of the EOS and  
 84 sound speed existence) resulting in hyperbolicity. In the basic flow model version  
 85 we address items (a) and (b) that are the most challenging. The model we address  
 86 considers mixtures and material interfaces in:

- 87 • velocity and pressure equilibrium (mechanical equilibrium),
- 88 • temperature equilibrium (thermal equilibrium).

89 This set of constraints is obviously valid in pure phases. In two-phase mixtures it  
 90 assumes that velocity slip is absent and that the mixing is fine enough to reach  
 91 temperature equilibrium. It means that the two-phase mixture is made of small  
 92 drops, small bubbles or foams. Experimental observations of cavitating and flashing  
 93 flows near macroscopic interfaces support these assumptions (Simoes-Moreira and  
 94 Shepherd 1999). From these assumptions it is possible to reduce non-equilibrium  
 95 two-phase flow models to mechanical and thermal equilibrium one. Such reduction  
 96 method is addressed in Kapila et al. (2001), Murrone and Guillard (2005), Saurel  
 97 et al. (2008), Lund (2012), Le Martelot et al. (2014) in various contexts. When both  
 98 mechanical and thermal relaxation are assumed to be stiff, it results in the following  
 99 system of partial differential equations:

$$\begin{aligned}
100 \quad & \frac{\partial(\alpha\rho)_1}{\partial t} + \operatorname{div}((\alpha\rho)_1\mathbf{u}) = 0, \quad \text{or alternatively} \quad \frac{\partial\rho}{\partial t} + \operatorname{div}(\rho\mathbf{u}) = 0 \\
101 \quad & \frac{\partial(\alpha\rho)_2}{\partial t} + \operatorname{div}((\alpha\rho)_2\mathbf{u}) = 0 \quad \frac{\partial\rho Y_1}{\partial t} + \operatorname{div}(\rho Y_1\mathbf{u}) = 0 \\
102 \quad & \frac{\partial\rho\mathbf{u}}{\partial t} + \operatorname{div}(\rho\mathbf{u} \otimes \mathbf{u} + p\mathbf{I}) = 0 \\
103 \quad & \frac{\partial\rho E}{\partial t} + \operatorname{div}((\rho E + p)\mathbf{u}) = 0 \quad (1) \\
104
\end{aligned}$$

105 where  $\alpha_k$ ,  $Y_k$ ,  $\rho_k$  ( $k = 1, 2$ ) denote respectively the volume fraction, the mass fraction  
106 and the material density.  $\rho$  represents the mixture density ( $\rho = \alpha_1\rho_1 + \alpha_2\rho_2$ ),  $\mathbf{u}$   
107 represents the centre of mass velocity,  $p$  denotes the pressure and  $E$  the mixture total  
108 energy ( $E = e + u^2/2$ ). The mixture internal energy is defined as  $e = Y_1e_1 + Y_2e_2$ .

109 System (1) is clearly reminiscent of the reactive (or multi-component) Euler equations  
110 widely used in chemically reacting flows. However, the thermodynamic closure  
111 departs significantly of the one used in gas mixtures. Indeed, in the present context  
112 it results from the following algebraic system:

$$113 \quad \begin{cases} T_1 = T_2 = T, \\ e = Y_1e_1(T, p) + Y_2e_2(T, p), \\ p_1 = p_2 = p, \\ \alpha_1 + \alpha_2 = 1 \text{ or alternatively, } Y_1v_1(T, p) + Y_2v_2(T, p) = v \end{cases} \quad (2)$$

114 In this algebraic system, the phases are in pressure equilibrium and each one occupies  
115 its own sub-volume or volume fraction  $\alpha_k$ . System (2) corresponds to a nonlinear  
116 system of two equations with the two unknowns  $T$  and  $p$ . To determine its explicit  
117 solution, EOS for the phases have to be provided. This is addressed in the forthcoming  
118 section. This thermodynamic closure differs significantly from that of ideal gas  
119 mixtures. In ideal mixtures each fluid occupies the entire volume, this assumption  
120 replacing the last equality of System (2). Also, the pressure is defined by the Dalton's  
121 law  $p = \sum_k p_k$  instead of the pressure equilibrium condition. In formulation (1) with  
122 thermodynamic closure (2) each phase occupies its own volume (and not the entire  
123 one) and evolves in temperature and pressure equilibrium with the other phase.

124 At interfaces separating pure liquid and pure gas the assumption of single temperature  
125 seems unrealistic as interface conditions, in the absence of mass transfer  
126 and heat diffusion, reduce to normal equal velocities and equal pressures, implying  
127 arbitrary temperature jumps. However, when heat diffusion is present an additional  
128 interface condition appears, corresponding to temperatures equality. Thus System  
129 (2) is valid for the computation of interfacial flows when:

- 130 • Heat diffusion is present and when it is possible to resolve the heat diffusion layer,  
131 as for example in the boiling flow configurations that will be considered latter.  
132 This is similar to laminar flames computations.

- 133 • A mushy zone is present at the interface. This is the case for example with flash-  
 134 ing and super-cavitating flows where the interface is not a clear discontinuity but a  
 135 sharp mixture layer in which thermodynamic relaxation and heat exchanges occur  
 136 intensively. This is similar to turbulent flames computations, where it is not possi-  
 137 ble to resolve all heat diffusion and chemical relaxation layers at subscale, but for  
 138 which ‘turbulent heat conduction’ imply global turbulent flame propagation.

139 System (1) with closure (2) is thus valid for the computation of:

- 140 • local interface dynamics when heat transfer is considered (this effect will be  
 141 inserted later),  
 142 • global (or macro-scale) interface dynamics when a micro-scale or subscale struc-  
 143 ture such as a mushy zone is present. Indeed, at subscale, heat transfer is neces-  
 144 sarily present, imposing temperature equality at the interface.

145 When phase transition is addressed Gibbs free energy relaxation terms have to be  
 146 considered in one of the mass equations:

$$147 \quad \frac{\partial \rho Y_1}{\partial t} + \frac{\partial \rho u Y_1}{\partial x} = \rho \nu (g_2 - g_1) \quad (3)$$

148 where  $g_k = h_k - T s_k$  denotes the phase k Gibbs free energy.  $h_k$  and  $s_k$  represent the  
 149 specific enthalpy and specific entropy.  $\nu$  represents a relaxation parameter that con-  
 150 trols the rate at which thermodynamic equilibrium is reached. The way this relax-  
 151 ation parameter is estimated will be addressed later. The entropy equation associated  
 152 to System (1)–(3) reads,

$$153 \quad \frac{\partial \rho s}{\partial t} + \frac{\partial \rho s u}{\partial x} = \frac{\rho \nu (g_2 - g_1)^2}{T}, \quad (4)$$

154 with the following definition for the mixture entropy:  $s = Y_1 s_1 + Y_2 s_2$ .

155 The same type of remark as before with temperature equality at interfaces is  
 156 needed to explain the validity of a single velocity model to compute interfacial flows  
 157 with phase transition. When heat diffusion and Gibbs energy relaxation are addressed  
 158 and solved at the interface, i.e., when the interface structure is solved, three velocities  
 159 appear at the global scale even if a single local velocity is present in the flow model.  
 160 The three velocities that appear at the global scale are the liquid one, the vapour one  
 161 and the phase transition front one.

162 This is similar to flames computation in which the reactive Navier–Stokes equa-  
 163 tions are appropriate to compute the reacting and burnt gas dynamics as well as flame  
 164 front dynamics.

165 The model has been shown to converge to exact sharp interface solutions in  
 166 Le Martelot et al. (2014). When the interface has more complex structure with tur-  
 167 bulent mixing at subscale, the same three velocities appear with different dynamics.  
 168 This is a consequence of turbulent heat diffusion and effective properties of fluid  
 169 media. In the limit, when flash evaporation is considered, the front velocity doesn’t

170 exceed the acoustic wave speed of System (1) or its thermodynamic equilibrium ana-  
 171 logue when the relaxation parameter  $\nu$  in Eq. (3) tends to infinity. Indeed, metastable  
 172 liquid is produced at a rate controlled by expansion waves, themselves propagating  
 173 at the speed of acoustic waves (Saurel et al. 2008). In this limit, the deflagration  
 174 speed of Chapman-Jouguet (Chaves 1984) is recovered as kinetic relation for the  
 175 global phase change front velocity. To summarize the discussion on the validity of  
 176 flow model (1), it is unable to compute accurately interfaces of simple mechanical  
 177 contact but it becomes valid:

- 178 • when heat conduction is considered and the interface structure is resolved, as done  
 179 for boiling flows (Le Martelot et al. 2014),
- 180 • when phase change occurs through interfaces with subscale structure, such as cav-  
 181 ating and flashing flows (Saurel et al. 2008; Le Martelot et al. 2013).

182 For practical use of System (1)–(2), EOSs have to be specified for the various  
 183 phases. This is the aim of the next section.

## 184 2.1 Equations of State

185 Phase transition and equations of state is a long lasting challenge.

### 186 About the van der Waal EOS

187  
 188  
 189 As mentioned in the introduction, the Cahn-Hilliard (1958) approach is quite popular  
 190 with boiling flows modelling, not with cavitating ones. It uses the van der Waals  
 191 (VdW) equation of state (EOS) to compute the pressure. This EOS provides the  
 192 pressure for the liquid phase, the gas phase and the two-phase mixture. It reads,

$$193 \quad p = \frac{\rho RT}{1 - \rho b} - c\rho^2 \quad (5)$$

194 where  $R$  denote the specific gas constant ( $R = \frac{r}{W}$ ) with  $r = 8.314$  J/mol/K and  
 195  $W$  (kg/mol) the molar mass.  $b$  represents the specific covolume, i.e. the volume occu-  
 196 pied by the molecules ( $\text{m}^3/\text{kg}$ ) and  $c$  is a constant associated to attractive effects.

197 This EOS contains a fundamental drawback schematized in Fig. 1 where an isen-  
 198 trope for the VdW EOS is shown.

199 EOS (5) thus presents unphysical behaviour during the phase change process. The  
 200 following interpretations follow:

- 201 • Equation (5) is aimed to close the balance equations of mass, momentum and  
 202 energy of the mixture. Unlike System (1), the volume or mass concentrations are  
 203 not considered in such formulations. A possible reason for choosing models with  
 204 three equations only is that adding a concentration equation requires additional



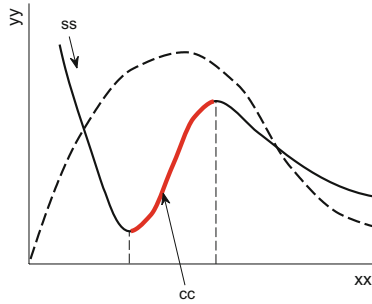


**Fig. 1** Thermodynamic path along an isentrope showing an expansion process starting from a pure liquid to the pure vapour region. The square sound speed  $c^2 = -v^2 \frac{\partial p}{\partial v}_s$  is well defined in the pure liquid and pure gas but is undefined in the two-phase region, between the metastable liquid and the metastable gas

205 information, such as the thermo-chemical relaxation rate  $\nu$ . These options, how-  
 206 ever, lead to the loss of hyperbolicity.

- 207 • In the VdW representation, phase transition is modelled as a thermodynamic path  
 208 and not as a kinetic one. Consequently the time variable is obviously absent in the  
 209 EOS. However, phase transition is a time delayed phenomenon and a thermody-  
 210 namic path seems a crude representation.

211 These remarks naturally lead us to the following thermodynamic closure, based  
 212 on three parameters  $P(\rho, e, Y)$  instead of two  $P(\rho, e)$  in the Van der Waals approach.

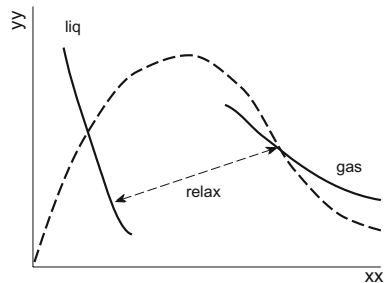
213

214 **EOS for pure fluids**

215

216 In the following we adopt an approach where each phase has its own EOS, each  
 217 EOS being thermodynamically consistent (convex) with well defined sound speed.  
 218 The connexion between the two phases is done through a kinetic path instead of a  
 219 thermodynamic one. Determination of the kinetic relaxation rate will be addressed  
 220 later. Schematic representation of the thermo-kinetic approach of phase transition is  
 221 shown in Fig. 2. This idea was promoted by Saurel et al. (2008).

**Fig. 2** Liquid and gas isentropes are connected through a kinetic path (Gibbs free energy relaxation process) during phase change



In this frame, liquid and gas require their own EOS, these ones being linked by the phase diagram. The building of such EOS has been addressed in Le Métayer et al. (2004) on the basis of the stiffened gas (SG) EOS. The main formulas for this EOS read for a given phase  $k = 1, 2$ :

$$\begin{aligned}
 p_k(\rho_k, e_k) &= \rho_k(\gamma_k - 1)(e_k - q_k) - \gamma_k p_{\infty k}, \\
 T_k(p_k, \rho_k) &= \frac{p_k + p_{\infty k}}{\rho_k C_{vk}(\gamma_k - 1)}, \\
 g_k(p_k, T_k) &= (\gamma_k C_{vk} - q'_k)T_k - C_{vk}T_k \ln \frac{T_k^{\gamma_k}}{(p_k + p_{\infty k})^{\gamma_k - 1}} + q_k.
 \end{aligned} \tag{6}$$

For a given phase, the following parameters are needed:  $\gamma_k$ ,  $p_{\infty k}$ ,  $C_{vk}$ ,  $q_k$ , and  $q'_k$ . As shown by Le Métayer et al. (2004) there is no difficulty to determine these parameters once the saturation curves for the liquid and gas are known. For liquid water and steam, the fluid parameters, optimized in the [300–500 K] temperature range, are the following:

*Liquid water:*

$$\begin{aligned}
 \gamma_{liq} &= 2.62 & P_{\infty, liq} &= 9058.29 \times 10^5 \text{ Pa} & C_{v, liq} &= 1606.97 \text{ J} \cdot \text{kg}^{-1} \cdot \text{K}^{-1} \\
 q_{liq} &= -1.150975 \times 10^6 \text{ J}
 \end{aligned}$$

*Water vapour:*

$$\begin{aligned}
 \gamma_{vap} &= 1.38 & P_{\infty, vap} &= 0 \text{ Pa} & C_{v, vap} &= 1192.51 \text{ J} \cdot \text{kg}^{-1} \cdot \text{K}^{-1} \\
 q_{vap} &= 2.060759 \times 10^6 \text{ J}
 \end{aligned}$$

These parameters are used in the computational examples of boiling and cavitating flows.

Expressing the thermal EOS of System (6) differently the following relation appears:

$$p_k(\rho_k, T_k) = \rho_k(\gamma_k - 1)C_{vk}T_k - p_{\infty k}. \tag{7}$$

The agitation part is  $\rho_k(\gamma_k - 1)C_{vk}T_k$  and is similar to the  $\rho RT$  part of (5). The attractive part ( $-p_{\infty k}$ ) is here a constant while it is density varying with the VdW EOS. The repulsive part  $(1 - \rho b)^{-1}$  is neglected in the SG formulation. Its consideration is addressed in Le Métayer and Saurel (2015).

The sound speed of a given phase reads,

$$c_k = \sqrt{\gamma_k \frac{p_k + p_{\infty k}}{\rho_k}}. \tag{8}$$

253 With this formulation the phases sound speed are always defined as  $p_k > -p_{\infty k}$ . Hav-  
 254 ing in hands EOS (6) for each phase we now address building of the EOS for the  
 255 mixture.

### 256 Mixture EOS

258 The mixture EOS is the one that closes System (1) with the help of mixture rules (2)  
 259 on the basis of formulation (6) for each phase. The algebraic system to solve is thus,  
 260

$$261 \quad e = Y_1 e_1(T, p) + Y_2 e_2(T, p),$$

$$262 \quad v = Y_1 v_1(T, p) + Y_2 v_2(T, p), \quad (9)$$

263 where  $e$  and  $v$  are obtained from the resolution of (1) and combination of the mass,  
 264 momentum and energy equations. The unknowns in (9) are consequently the mixture  
 265 temperature  $T$  and pressure  $P$ . Combining the caloric and thermal EOSs of (6) the  
 266 energy for a given phase reads,

$$267 \quad e_k(T_k, p_k) = C_{vk} T_k + p_{\infty k} \rho_k / q_k.$$

268 Inserting this expression in the first equation of (6) the specific volume as a function  
 269 of pressure and temperature is obtained:

$$270 \quad v_k(T_k, p_k) = \frac{(\gamma_k - 1) C_{vk} T_k}{p_k + p_{\infty k}}. \quad (10)$$

271 Inserting this expression in one of the EOS (6) the internal energy as a function of  
 272 pressure and temperature is obtained:

$$273 \quad e_k(T_k, p_k) = \frac{(p_k + \gamma_k p_{\infty k}) C_{vk} T_k}{p_k + p_{\infty k}} + q_k.$$

274 With these definitions, System (9) becomes,

$$275 \quad T(e, p, Y_1) = (e - \bar{q}) \left( \sum_i \frac{Y_i C_{vi} (p + \gamma_i p_{\infty i})}{p + p_{\infty i}} \right)^{-1}, \quad (11)$$

$$276 \quad T(v, p, Y_1) = v \left( \sum_i \frac{(\gamma_i - 1) Y_i C_{vi}}{p + p_{\infty i}} \right)^{-1}, \quad (12)$$

277 with  $\bar{q} = Y_1 q_1 + Y_2 q_2$ .

278 Eliminating the temperature from these two equations the EOS for the pressure  
 279 is obtained as solution of the following quadratic equation:

$$280 \quad a_2 p^2 + a_1 p + a_0 = 0$$

$$\begin{aligned}
 282 \quad a_2 &= Y_1 C_{v1} + Y_2 C_{v2} \\
 283 \quad a_1 &= Y_1 C_{v1} (p_{\infty 2} + \gamma_1 p_{\infty 1} - (\gamma_1 - 1)Q) + Y_2 C_{v2} (p_{\infty 1} + \gamma_2 p_{\infty 2} - (\gamma_2 - 1)Q) \\
 284 \quad a_0 &= -Q((\gamma_1 - 1)Y_1 C_{v1} p_{\infty 2} + (\gamma_2 - 1)Y_2 C_{v2} p_{\infty 1}) + p_{\infty 1} p_{\infty 2} (\gamma_1 Y_1 C_{v1} + \gamma_2 Y_2 C_{v2})
 \end{aligned}$$

285 where

$$286 \quad Q = \rho(e - \bar{q})$$

287 The pressure is given by the only positive root:

$$288 \quad p = \frac{-a_1 + \sqrt{a_1^2 - 4a_0a_2}}{2a_2} \quad (13)$$

289 Once the pressure is determined, the temperature is computed by either (11) or  
 290 (12). The mixture sound speed has a non-monotonic behaviour versus the volume  
 291 fraction as shown in Fig. 4.

292 From the results shown in Fig. 3 it appears that there is no practical need to com-  
 293 pute the mixture sound speed that is quite complex and computationally expensive  
 294 (its explicit expression is given in Le Martelot et al. (2014)). As it is always lower  
 295 than the mechanical equilibrium one, this one is preferred in the numerical computa-  
 296 tions, as better stability is guaranteed with this estimate. The mechanical equilibrium  
 297 sound speed obeys the well known Wood (1930) formula:

$$298 \quad \frac{1}{\rho c_w^2} = \frac{\alpha_1}{\rho_1 c_1^2} + \frac{\alpha_2}{\rho_2 c_2^2} \quad (14)$$

299 The volume fractions are determined from the resolution of System (1) and the spe-  
 300 cific volumes computed by (10) with the pressure given by (13) and temperature  
 301 given by (12). The phase sound speeds are given by (8).

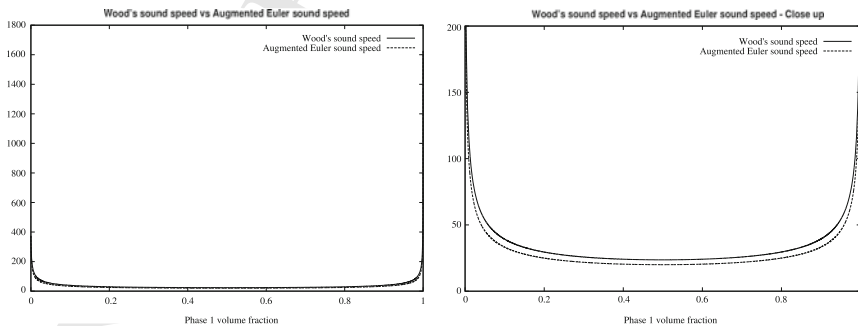


**Fig. 3** Representation of the mechanical equilibrium mixture sound speed (in *lines*) and the pressure-temperature equilibrium mixture sound speed (in *dashed lines*). Both sound speeds present a non-monotonic behaviour versus volume fraction. The mechanical equilibrium sound speed is always slightly higher than the pressure-temperature equilibrium one

### 3 Kinetic Relaxation Rate—Thermo-Chemical Relaxation Solver

When dealing with phase transition the relaxation rate  $\nu$  present in the concentration equation (3) has to be specified. Following Saurel et al. (2008), the guess  $\nu \rightarrow \infty$  is appropriate in most situations. In other words, pure liquid and pure gas are allowed to have any temperature during the hyperbolic step and instantly reach thermodynamic equilibrium at the saturation conditions where both liquid and gas are present (interface and mixture zones). This assertion is justified as follows:

- When dealing with the direct numerical simulation of boiling flows, the fluids become metastable as a consequence of heat diffusion. Heat conduction is slow and controls the global rate of phase change. Thus, one can assume that phase transition occurs at any rate, given it is greater than heat conduction. For the sake of simplicity, infinitely fast relaxation is adopted.
- When dealing with cavitating flows, it is assumed that the fluids contain enough impurities to have many nucleation sites. Around evaporating interfaces, phase transition happens and their collective effects result in macroscopic cavitation fronts surrounded by mushy zones. In these mushy zones the interfacial area is so large that heat and mass exchange are intense enough so that a flow model with a unique temperature and stiff Gibbs energy relaxation is appropriate.
- When none of the fluids is metastable (pure liquid state and pure gas state) no thermo-chemical relaxation occurs and the flow model reduces to single phase equations, with appropriate thermodynamics.

With this approach the thermodynamic path that the fluid follows during an isentropic expansion is shown in Fig. 4.

As the thermo-chemical solver is used as soon as metastable states appear, the effective thermodynamic path that the fluid follows is that of Fig. 4. Such a path could be reproduced by a reduced version of the flow model (1) with three equations only (mixture mass, mixture momentum and mixture energy). However, the sound speed

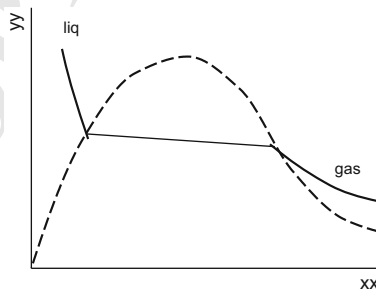


**Fig. 4** As metastable states are transformed stiffly to equilibrium mixture states the effective thermodynamic path corresponds in the two-phase region to a line whose slope has been exaggerated in the figure. The slope is non zero but is weak, as sound propagates slowly in two-phase mixtures

of such a model is not convenient, as it is costly to compute, and most importantly, discontinuous at the phase diagram boundaries.

Here, the flow model has a sound speed always defined and continuous. As mentioned earlier, Eq. (14) is a fair approximation. Also, extending System (1) to the presence of non-condensable gas is straightforward while it is non-trivial with a more reduced model.

The presence of a stiff relaxation term in (3) does not result in computational difficulties as integration of such term is never addressed: in the following, only the equilibrium state is required.

The relaxed solution corresponding to thermodynamic equilibrium is obtained considering the mixture mass and mixture energy definition:

$$v = \frac{1}{\rho} = Y_1 v_1 + Y_2 v_2 = cst = v_0 \quad (15)$$

$$e = Y_1 e_1 + Y_2 e_2 = cst = e_0 \quad (16)$$

where  $Y_1 = \frac{\alpha_1 \rho_1}{\rho}$  and  $Y_2 = \frac{\alpha_2 \rho_2}{\rho} = 1 - Y_1$  are the varying mass fractions of both phases. In the following the liquid and its vapour are denoted respectively by the subscripts '1' and '2'.

The specific volumes and internal energies are given by the SG EOS:

$$v_k = \frac{(\gamma_k - 1) C_{vk} T_k}{p_k + p_{\infty,k}}, \quad (17)$$

$$e_k = C_{vk} T_k \left( 1 + \frac{(\gamma_k - 1) p_{\infty,k}}{p_k + p_{\infty,k}} \right) + q_k. \quad (18)$$

All parameters appearing in relations (17), (18) and (19) are computed in order to satisfy the experimental liquid/vapour saturation curves (Le Métayer et al. 2004).

The final relaxed state, denoted by the superscript '\*' corresponds to the thermodynamic equilibrium state. The liquid and vapour phases have a common pressure, temperature and Gibbs free energy. Equality of Gibbs free energy of both phases,

$$g_k = h_k - T_k s_k = (\gamma_k C_{vk} - q'_k) T_k - C_{vk} T_k \ln \frac{T_k^{\gamma_k}}{(p + p_{\infty,k})^{\gamma_k - 1}} + b_k P_k + q_k, \quad (19)$$

provides a relation between the pressure and the temperature:

$$T^*(p^*) = T_{sat}(p^*) \quad (20)$$

This relation represents the evolution of the saturation temperature as a function of pressure. Thanks to (20), the relation (15) reads,

$$v_0 = Y_1^* v_1^*(p^*) + Y_2^* v_2^*(p^*) = Y_1^* v_1^*(p^*) + (1 - Y_1^*) v_2^*(p^*), \quad (21)$$

with,

$$v_k^*(p^*) = \frac{(\gamma_k - 1)C_{vk}T^*(p^*)}{p^* + p_{\infty,k}}. \quad (22)$$

Variables  $v_1^*$  and  $v_2^*$  thus correspond to the saturated specific volumes of the liquid and vapour phases respectively.

A first relation linking the liquid mass fraction and the pressure is obtained from (21):

$$Y_1^* = \frac{v_2^*(p^*) - v_0}{v_2^*(p^*) - v_1^*(p^*)}. \quad (23)$$

In relation (23) the existence of physical solution is fulfilled by the following condition:

$$0 < Y_1^* < 1 \Leftrightarrow v_1^*(p^*) < v_0 < v_2^*(p^*) \quad (24)$$

By using once more the saturation relation (20), the total energy equation (16) becomes,

$$e_0 = Y_1^* e_1^*(p^*) + Y_2^* e_2^*(p^*) = Y_1^* e_1^*(p^*) + (1 - Y_1^*) e_2^*(p^*), \quad (25)$$

where,

$$e_k^*(p^*) = C_{vk}T^*(p^*) \left( 1 + \frac{(\gamma_k - 1)p_{\infty,k}}{p^* + p_{\infty,k}} \right) + q_k. \quad (26)$$

A second relation linking the liquid mass fraction and the final pressure is obtained,

$$Y_1^* = \frac{e_0 - e_2^*(p^*)}{e_1^*(p^*) - e_2^*(p^*)}. \quad (27)$$

It is more convenient to rewrite relation (27) in terms of specific enthalpies by combining (21) and (25),

$$e_0 + p^* v_0 = Y_1^* (e_1^*(p^*) + p^* v_1^*(p^*)) + Y_2^* (e_2^*(p^*) + p^* v_2^*(p^*)) = Y_1^* h_1^*(p^*) + Y_2^* h_2^*(p^*), \quad (28)$$

which directly introduces the latent heat of vaporization  $L_v(p^*)$ ,

$$L_v(p^*) = h_2^*(p^*) - h_1^*(p^*). \quad (29)$$

Equation (27) then becomes:

$$Y_1^* = \frac{h_2^*(p^*) - (e_0 + p^* v_0)}{h_2^*(p^*) - h_1^*(p^*)}. \quad (30)$$

386 In relation (30) a second existence condition appears,

$$387 \quad 0 < Y_1^* < 1 \Leftrightarrow h_1^*(p^*) < e_0 + p^* v_0 < h_2^*(p^*). \quad (31)$$

388 Equating relations (23) and (30) leads to an equation where the final pressure  $p^*$  is  
389 the only unknown,

$$390 \quad \frac{h_2^*(p^*) - (e_0 + p^* v_0)}{h_2^*(p^*) - h_1^*(p^*)} - \frac{v_2^*(p^*) - v_0}{v_2^*(p^*) - v_1^*(p^*)} = 0. \quad (32)$$

391 Once the solution of (32) is obtained—through Newton’s method for instance—the  
392 other thermodynamic variables are easily obtained by the preceding relations pre-  
393 sented above.

394 However Eq. (32) may not provide a physical solution depending on the initial energy  
395  $e_0$  and specific volume  $v_0$ . This is the case when conditions (24) and (31) are not ful-  
396 filled. In such instances the liquid/vapour system tends towards a final state where  
397 a single phase is present. Total evaporation or condensation thus occurs during the  
398 relaxation process, and the corresponding thermodynamic state is computed with  
399 Eq. (13) where the mass fraction of one of the phases has been set to 1.

## 400 4 Hyperbolic Solver

401 For the sake of simplicity, the presentation of the solver is one-dimensional, and  
402 limited to first order. Details about higher order extensions may be found in Toro  
403 (2009).

404 System (1) is written in compact form as,

$$405 \quad \frac{\partial U}{\partial t} + \frac{\partial F(U)}{\partial x} = 0, \quad (33)$$

406 where  $U = [\rho \ \rho u \ \rho E \ \rho Y]^t$  is the conservative variables vector, and  $F =$   
407  $[\rho u \ \rho u^2 + p \ (\rho E + p)u \ \rho u Y]^t$  represents the associated flux vector.

### 408 Godunov scheme

409 System (33) is a hyperbolic system of conservation laws, with wave speeds  $u, u - c_{eq}$   
410 and  $u + c_{eq}$ .

411 The first-order Godunov method reads,

$$412 \quad U_i^{n+1} = U_i^n - \frac{\Delta t}{\Delta x} (F_{i+1/2}^* - F_{i-1/2}^*), \quad (34)$$



416 under the CFL stability condition,

417 
$$\Delta t \leq \frac{\Delta x}{\max(u \pm c_{eq})}. \tag{35}$$

418 The cell boundary fluxes  $F_{i\pm 1/2}$  are computed with the following approximate  
 419 solver.

420  
 421 **HLLC solver**

422  
 423 The HLLC solver (Toro et al. 1994) is an approximate Riemann solver for the Euler  
 424 equations that is easy to adapt to the present “real gas” context. In the HLLC context,  
 425 each wave is considered as a discontinuity:

- 426 • a contact discontinuity wave, with characteristic speed  $S_M$ , through which pressure  
 427 and velocity is constant  
 428 • two discontinuities, with characteristic speed  $S_L$  and  $S_R$  (left facing and right facing  
 429 waves), through which mass fractions  $Y_i$  are constant.

430 As shown in Fig. 5, each of these waves separate the states:  $(\bar{U}_L, \bar{U}_L^*, \bar{U}_R^*, \bar{U}_R)$ , from  
 431 which it is possible to compute the appropriate flux between the two cells during the  
 432 time step.

433 In the example depicted in Fig. 5,  $U_L^*$  is the appropriate state to compute the inter-  
 434 cell flux  $F$ , since it is the state which persists at the physical position of the cell  
 435 discontinuity during the time step. In a more general context, there are four possible  
 436 cases depending on the signs of the three wave velocities:

- 437 case a  $S_L > 0 \rightarrow F = F(U_L)$   
 438 case b  $S_R < 0 \rightarrow F = F(U_R)$   
 439 case c  $S_M > 0, S_L < 0 \rightarrow F = F(U_L^*)$   
 440 case d  $S_M < 0, S_R > 0 \rightarrow F = F(U_R^*)$

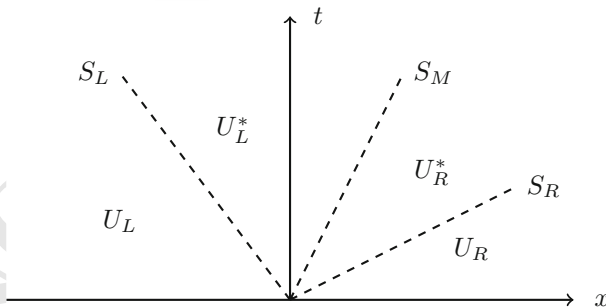


**Fig. 5** Schematic representation of the Riemann problem emerging at each cell boundary. Three nonlinear waves are emitted, each one being considered as a discontinuity

## 441 Wave speeds estimates and fluxes computation

442

443 Following Davis (1988), the right and left waves velocities can be approximated as,

$$444 \quad S_R = \max((u + c_w)_R, (u + c_w)_L), \quad (36)$$

$$445 \quad S_L = \min((u - c_w)_R, (u - c_w)_L). \quad (37)$$

446 Knowledge of  $c_{eq}$  is not required as it is replaced everywhere by its approximation  
447  $c_w$  in the solver that follows.

448 Each discontinuity obeys the Rankine-Hugoniot conditions given by:

$$449 \quad [F] - S_k[U] = 0 \quad (38)$$

450 where  $S_k$  denotes the speed of the  $k$ th discontinuity and [...] denotes the jump of a  
451 given variable across the discontinuity.

452 Under HLL approximation, the intermediate wave speed is given by

$$453 \quad S_M = u^* = \frac{p_R - p_L + \rho_R u_R (u_R - S_R) - \rho_L u_L (u_L - S_L)}{\rho_R (u_R - S_R) - \rho_L (u_L - S_L)} \quad (39)$$

454 Using again the Rankine-Hugoniot jump conditions, one can derive the following  
455 relations for the intermediate state:

$$456 \quad \begin{cases} \rho_R^* = \rho_R \frac{u_R - S_R}{S_M - S_R} \\ u_R^* = u^* = S_M \\ p_R^* = p_R + \rho_R (u_R - S_R)(u_R - S_M) \\ E_R^* = E_R + \frac{p_R (u_R - S_M)}{\rho_R (u_R - S_R)} - S_M (u_R - S_M) \\ Y_{R,i}^* = Y_{R,i} \end{cases} \quad (40)$$

457 These relations fully define the intercell set of conservative variables  $U_R^*$ , and con-  
458 sequently the flux  $F(U_R^*)$  given by,

$$459 \quad F_R^* = F_R - S_R (U_R - U_R^*). \quad (41)$$

460 Substituting the  $L$  index to the  $R$  index in the above formula leads to a similar expres-  
461 sion for the remaining flux  $F(U_L^*)$ .

462 The computational examples that follow were achieved with the DALPHADT  
463 code based on tetrahedron meshes. In this frame, the Godunov method reads,

$$464 \quad U_{k,i}^{n+1} = U_{k,i}^{n+1} - \frac{\Delta t}{V_i} \sum_{f=1}^4 (F_k^* \cdot \vec{\eta})_f S_f, \quad (42)$$

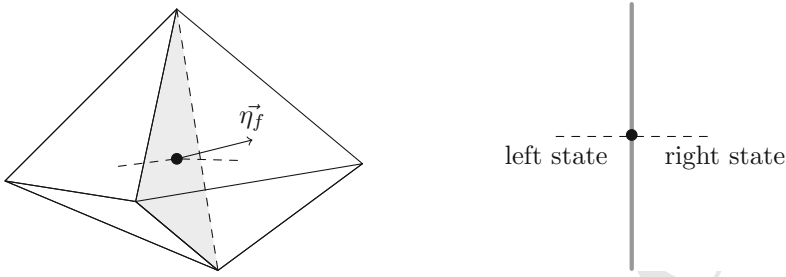


**Fig. 6** 3D Godunov method applied to computational control volumes made of tetrahedrons. The code is cell-centered, and the Riemann problem is solved at each face. ▲ tetrahedron center. • face center

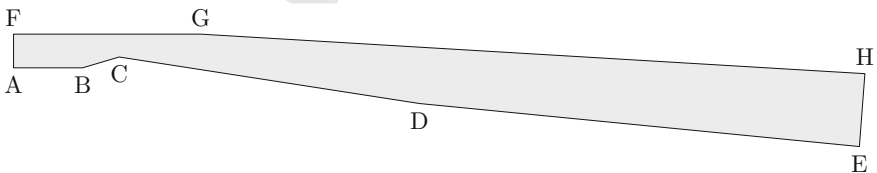
465 where  $S_f$  is the face area, and  $(F_k^* \cdot \vec{\eta})_f$  represents the flux solution of the Riemann  
 466 problem solved along the face normal vector  $\vec{\eta}_f$  of a given face of the tetrahedron, as  
 467 illustrated in Fig. 6.

468 We now address computational examples.

## 469 5 Cavitating Flows

470 In this section, 2D two-phase flow computations in Venturi nozzle are addressed.  
 471 The configuration studied corresponds to the experimental facility built at LEGI  
 472 Laboratory in Grenoble, France by the group led by S. Barre. The test section  
 473 corresponds to a Venturi channel with a nozzle divergent inclined at an angle of  $8^\circ$ .  
 474 The geometry is shown in Fig. 7.

475 The fluids considered correspond to liquid and vapour water, with the equation of  
 476 state parameters given in Sect. 2.1. The boundary conditions correspond to imposed



	X (abscissa) (m)	Y (m)		X(abscissa) (m)	Y (m)
A	0	0	E	1.225	-0.114
B	0.1	0	F	0	0.0488
C	0.153	0.0157	G	0.271	0.0488
D	0.588	-0.0517	H	1.233	-0.00845

**Fig. 7** Geometrical data of the Venturi  $8^\circ$  nozzle of LEGI, France

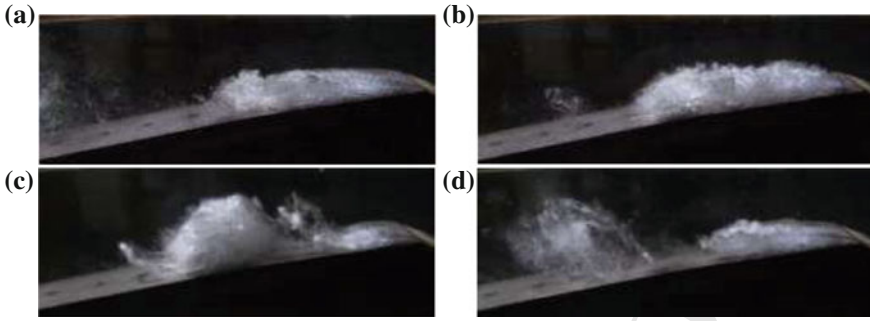


**Fig. 8** Experimental photographs of the break off cycle observed in the 8° Venturi nozzle with the boundary conditions aforementioned. Flow direction is from right to left. A cavitation pocket appears, extends and separates in two sub-pockets, one transported with the mean flow and another one collapsing close to the nozzle. Courtesy of S. Barre (LEGI)

477 mass inflow with both imposed stagnation enthalpy and entropy at the inlet and pre-  
 478 scribed pressure at the outlet. The imposed conditions at the inlet are the following,

$$\left\{ \begin{array}{l} m = 7514.917 \text{ kg.m}^{-2}.\text{s}^{-1} \\ \rho_{liq} = 1067.56 \text{ kg.m}^{-3} \\ \rho_{vap} = 0.387 \text{ kg.m}^{-3} \\ \alpha_{liq} = 0.999 \\ P = 51825 \text{ Pa} \end{array} \right.$$

480 while, at the right outlet, the prescribed pressure is  $P = 72025 \text{ Pa}$ .

481 With these boundary conditions a periodic flow has been observed experimentally  
 482 as shown in the Fig. 8.

483 In the first stage of the cycle (a), a cavitation sheet is attached to the throat and grows.  
 484 In a second stage, the sheet reaches its maximum length (b) and breaks into two main  
 485 parts (c). At the end, the downstream part is swept along within the stream and starts  
 486 to collapse while the attached part starts another cycle (d). The mean attached cavity  
 487 length value is  $45 \pm 5 \text{ mm}$  while the quasi-periodic vapour cloud shedding frequency  
 488 is about 45 Hz.

489 To compute this unstable flow a 2D unstructured mesh containing 52450 cells is  
 490 used. The grid is refined at the throat in order to capture the cavitation pocket. The  
 491 average cell size is 0.013 mm at throat and 0.08 mm elsewhere.

492 The explicit scheme summarized in Sect. 4 is extended to time implicit integration  
 493 and the Riemann problem is preconditioned with the method detailed in Le Martelot  
 494 et al. (2013). The flow is computed during 1.8 s of physical time, this time being long  
 495 enough to obtain a quasi-stationary flow with quasi-periodic vapour clouds shedding.  
 496 An example of the obtained cloud shedding is shown in the volume fraction contours  
 of Fig. 9. Examining the water vapour volume fraction contours oscillations, we were

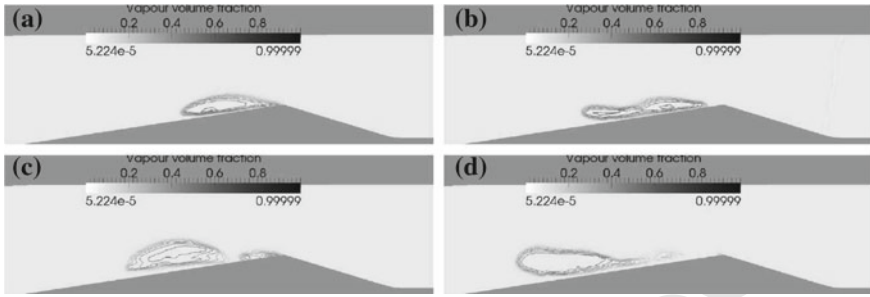


**Fig. 9** Computed volume fraction of water vapour. This example shows the same four different parts as those observed during the experimental studies and shown in Fig. 8. The mean attached cavity length is about 45 mm, in perfect agreement with the experiments

497 able to determine a vapour pocket shedding frequency of about 43 Hz, in excellent  
 498 agreement with the measured frequency for the pressure fluctuations (45 Hz.).

499 By performing measurements during every cycle, an average attached cavity  
 500 length of about 45 mm has been measured from the computations. These results  
 501 show very good agreement with the experiments. Indeed, experimental measure-  
 502 ments gave a mean attached cavity length equals to  $45 \pm 5$  mm.

503 These results show that it is possible to reproduce the large structures of such  
 504 cavitating flows with a flow model free of parameters. In particular, no turbulence  
 505 model is used.

## 506 6 Boiling Flows

507 To deal with DNS-type of boiling flows, System (1) has to be enhanced by introduc-  
 508 ing additional physical effects:

- 509 • buoyancy,
- 510 • surface tension,
- 511 • heat conduction.

512 Surface tension effects are considered through the Continuum Surface Force (CSF)  
 513 method of Brackbill et al. (1992). The capillary force is modelled as,

$$514 \quad \mathbf{F}_\sigma = \sigma \kappa \overline{\nabla Y_1} \quad (43)$$

515 where  $\sigma$  represents the surface tension coefficient ( $\text{N}\cdot\text{m}^{-1}$ ),  $\kappa$  represents the local  
 516 curvature ( $\text{m}^{-1}$ ) and  $Y_1$  is the mass fraction of phase 1. The local curvature reads,

$$517 \quad \kappa = -\text{div} \left( \frac{\overline{\nabla Y_1}}{|\overline{\nabla Y_1}|} \right). \quad (44)$$

518 The gravity force is modelled as,

$$519 \quad \mathbf{F}_g = \rho \mathbf{g},$$

520 where  $\mathbf{g}$  represents the gravity constant.

521 Heat conduction is inserted in the total energy equation of the model through the  
522 Fourier law  $\mathbf{q} = -\lambda_c \overline{\nabla T}$  where the ‘‘mixture’’ thermal conductivity is given by  $\lambda_c =$   
523  $\alpha_1 \lambda_1 + \alpha_2 \lambda_2$  and  $\lambda_k$  represents the thermal conductivity of phase  $k$ . Details are given  
524 in Le Martelot et al. (2014).

525 Inserting these extra effects, the flow model now becomes:

$$\begin{aligned} & \frac{\partial \rho Y_1}{\partial t} + \operatorname{div}(\rho Y_1 \mathbf{u}) = \rho \nu (g_2 - g_1) \\ & \frac{\partial \rho}{\partial t} + \operatorname{div}(\rho \mathbf{u}) = 0 \\ 526 \quad & \frac{\partial \rho \mathbf{u}}{\partial t} + \operatorname{div}(\rho \mathbf{u} \otimes \mathbf{u} + P \underline{\underline{I}}) = \sigma \kappa \overline{\nabla Y_1} + \rho \mathbf{g} \\ & \frac{\partial \rho E}{\partial t} + \operatorname{div}((\rho E + P)\mathbf{u}) = \operatorname{div}(\lambda_c \overline{\nabla T}) + \sigma \kappa \overline{\nabla Y_1} \cdot \mathbf{u} + \rho \mathbf{g} \cdot \mathbf{u} \end{aligned} \quad (45)$$

527 A conservative form is available as well,

$$\begin{aligned} & \frac{\partial \rho Y_1}{\partial t} + \operatorname{div}(\rho Y_1 \mathbf{u}) = \rho \nu (g_2 - g_1) \\ & \frac{\partial \rho}{\partial t} + \operatorname{div}(\rho \mathbf{u}) = 0 \\ 528 \quad & \frac{\partial \rho \mathbf{u}}{\partial t} + \operatorname{div}(\rho \mathbf{u} \otimes \mathbf{u} + P \underline{\underline{I}} - \sigma \underline{\underline{m}}) = \rho \mathbf{g} \\ & \frac{\partial \rho E + \sigma |\overline{\nabla Y_1}|}{\partial t} + \operatorname{div}((\rho E + P + \sigma |\overline{\nabla Y_1}|)\mathbf{u} - \sigma \underline{\underline{m}} \cdot \mathbf{u} - \lambda_c \overline{\nabla T}) = \rho \mathbf{g} \cdot \mathbf{u} \end{aligned} \quad (46)$$

$$529 \quad \text{where } \underline{\underline{m}} = \left( |\overline{\nabla Y_1}| \underline{\underline{I}} - \frac{\overline{\nabla Y_1} \otimes \overline{\nabla Y_1}}{|\overline{\nabla Y_1}|} \right).$$

530 This system is closed by the EOS (13). The entropy equation associated to System  
531 (45) reads,

$$532 \quad \frac{\partial \rho S}{\partial t} + \operatorname{div} \left( \rho S \mathbf{u} - \frac{\lambda_c \overline{\nabla T}}{T} \right) = \frac{\rho \nu (g_2 - g_1)^2}{T} + \lambda_c \frac{(\nabla T)^2}{T^2} \quad (47)$$

533 with  $S = Y_1 s_1 + Y_2 s_2$ , and shows agreement with the second law of thermodynam-  
534 ics, as the right hand side of (47) is positive.

535 System (46) is considered hereafter to compute boiling flow examples.

536

537 A closed and adiabatic rectangular domain ( $12\text{ cm} \times 7\text{ cm}$ ) in which the lower half  
 538 is filled with saturated liquid water and the upper half is filled with saturated vapour  
 539 is considered.

540 The surface tension coefficient is set to  $\sigma = 73 \cdot 10^{-3}\text{ N}\cdot\text{m}^{-1}$ , the contact angle is taken  
 541 constant and equal to  $\theta = 45^\circ$  and the gravity acceleration is set to  $|\mathbf{g}| = 9.81\text{ m}\cdot\text{s}^{-2}$ .

542 At start, the initial volume fraction of vapour is  $\alpha_{vap} = 0.0001$  in the lower  
 half domain and  $\alpha_{vap} = 0.9999$  in the upper part. Moreover, the initial pressure

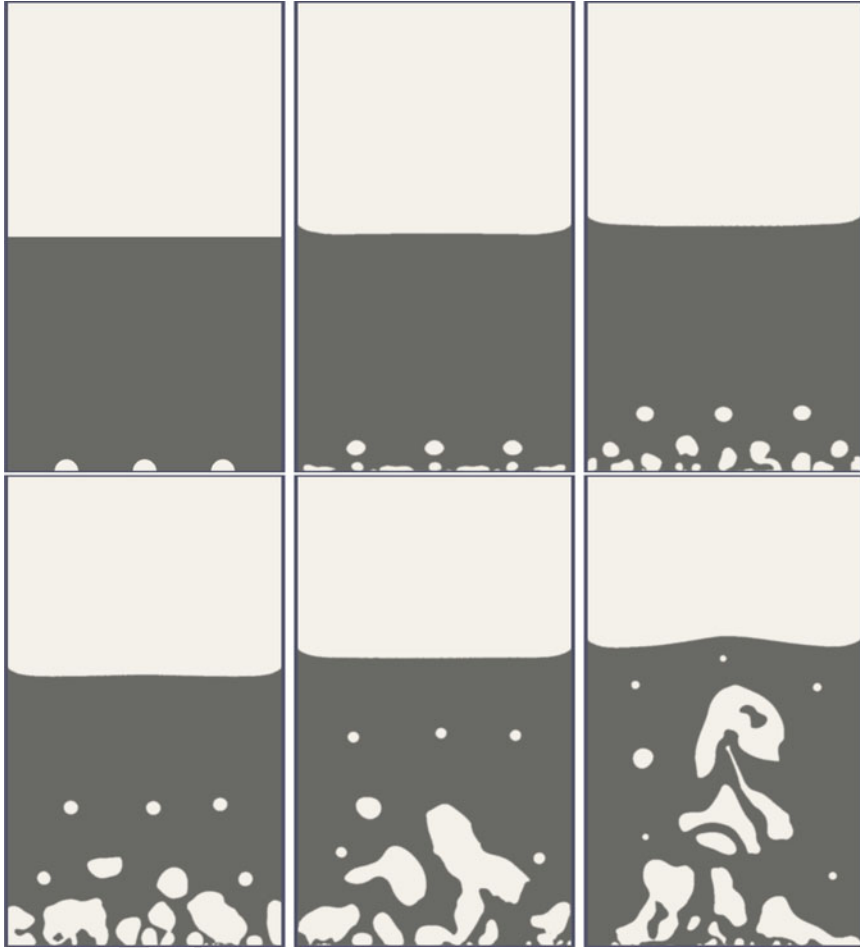


**Fig. 10** Vapour mass fraction contours at times  $t = 0\text{ s}$ ,  $t = 50\text{ ms}$ ,  $t = 100\text{ ms}$ ,  $t = 200\text{ ms}$ ,  $t = 300\text{ ms}$  and  $t = 400\text{ ms}$ . A vapour film appears at the first instants. As a result of wall effects combined with capillary ones a big elongated bubble is created at the centre and breaks up in several bubbles. New bubbles appear at the bottom wall as a consequence of wall heating

543 and temperature are initialised with the hydrostatic gravity profile with the con-  
 544 straint  $T = T_{SAT}(P)$  in each cell. The bottom wall temperature is set constant at  
 545  $T_{SAT}(P_{atm}) + 15K$ .

546 The numerical scheme presented in the former section is rendered time implicit and  
 547 the Riemann solver is low Mach pre-conditioned (Le Martelot et al. 2014). A mesh  
 548 made of  $960 \times 560$  cells is used in the computations that follow.

549 Three vapour bubbles (radius = 3 mm) are set initially at the bottom wall as shown  
 550 in the first image of Fig. 10. The volume fraction of vapour inside these bubbles is  
 551  $\alpha_{vap} = 0.9999$ . The computed vapour mass function is shown in the same figure.

552 The first instants show the three first bubbles moving toward the surface due to buoy-  
 553 ancy effects while, as the bottom wall of the box is heated, liquid water begins to boil,  
 554 creating a vapour film. The boiling phenomenon appears as consequence of wall  
 555 heating effect that renders the liquid locally slightly overheated. Indeed, the assump-  
 556 tion made is that the liquid contains enough impurities to not accept overheating,  
 557 as pure liquids are able to become metastable while real liquids are not. Therefore,  
 558 using the phase transition solver of Sect. 4 after checking that the liquid is not in  
 559 stable state, the equilibrium state is computed on the basis of Eq. (32) and a mixed  
 560 cell appears. From this “nucleation cell site” and merging effects due to surface ten-  
 561 sion, convection and inertia, new bubbles appear. Once created, these new bubbles  
 562 begin to rise and, as there is now again liquid in contact with the bottom wall, new  
 563 bubbles appear behind them and begin to grow.

564 It is worth to mention that the bottom wall of the box is a perfect surface, where  
 565 uniform temperature and constant contact angle are set. According to the velocity  
 566 profiles, the first bubbles seem to be created between the convective rolls, where the  
 567 velocity is the lowest, as shown in Fig. 10.

## 568 7 Conclusions

569 Boiling, evaporation and cavitation are essentially the same phenomenon, driven by  
 570 phase transition, but in different pressure and temperature conditions. Consequently,  
 571 they ought to be described by the same model, and deriving such a model is the object  
 572 of the present work. The flow model is essentially a hyperbolic system with relax-  
 573 ation terms. Coping with boiling, evaporation and cavitation, it is—in the authors  
 574 knowledge—the first approach showing such a wide range of applicability. It is also  
 575 a very robust computational approach of phase transition compared to existing alter-  
 576 natives. Although not shown here, our preliminary investigations show that the flow  
 577 model can be extended to cope not only with a liquid–vapour couple, but also with  
 578 multi-component gas mixtures.

579 **Acknowledgements** Part of this work has been carried out in the framework of the Labex MEC  
 580 (ANR-10-LABX-0092) and of the A\*MIDEX project (ANR-11-IDEX-0001-02), funded by the  
 581 Investissements d’Avenir French Government program managed by the French National Research  
 582 Agency (ANR). We also acknowledge funding from ANR through project ANR-14-CE22-0014. Pr.  
 583 Stéphane Barre (LEGI) is also gratefully acknowledged for providing the photographs of Fig. 8.



## References

- 584
- 585 Barre, S., Rolland, J., Boitel, G., Goncalves, E., & Fortes Patella, R. (2009). Experiments and mod-  
586 eling of cavitating flows in Venturi: Attached sheet cavitation. *European Journal of Mechanics-  
587 B/Fluids*, 280(3), 444–464.
- 588 Brackbill, J. U., Kothe, D. B., & Zemach, C. I. (1992). A continuum method for modeling surface  
589 tension. *Journal of Computational Physics*, 100(2), 335–354.
- 590 Cahn, J. W., & Hilliard, J. E. (1958). Free energy of a nonuniform system. I. Interfacial free energy.  
591 *The Journal of Chemical Physics*, 280(2), 258–267.
- 592 Chaves, H. (1984). Changes of phase and waves on depressurization of liquids with high specific  
593 heat. *NASA STI/Recon Technical Report N*, 84, 25003.
- 594 Coutier-Delgosha, O., Fortes-Patella, R., & Reboud, J.-C. (2003). Evaluation of the turbulence  
595 model influence on the numerical simulations of unsteady cavitation. *Journal of Fluids Engi-  
596 neering*, 1250(1), 38–45.
- 597 d’Agostino, L., & Salvetti, M. V. (2008). *Fluid dynamics of cavitation and cavitating turbopumps*  
598 (Vol. 496). Springer Science & Business Media.
- 599 Davis, S. F. (1988) Simplified second-order Godunov-type methods. *SIAM Journal on Scientific  
600 and Statistical Computing*, 90(3), 445–473.
- 601 Goncalves, E., & Patella, R. F. (2009). Numerical simulation of cavitating flows with homogeneous  
602 models. *Computers & Fluids*, 380(9), 1682–1696.
- 603 Jamet, D., Lebaigue, O., Coutris, N., & Delhaye, J. M. (2001). The second gradient method for the  
604 direct numerical simulation of liquid–vapor flows with phase change. *Journal of Computational  
605 Physics*, 1690(2), 624–651.
- 606 Kapila, A. K., Menikoff, R., Bdzil, J. B., Son, S. F., & Stewart, D. S. (2001). Two-phase modeling of  
607 deflagration-to-detonation transition in granular materials: Reduced equations. *Physics of Fluids  
608 (1994–present)*, 130(10), 3002–3024.
- 609 Le Martelot, S., Nkonga, B., & Saurel, R. (2013). Liquid and liquid-gas flows at all speeds. *Journal  
610 of Computational Physics*, 255, 53–82.
- 611 Le Martelot, S., Saurel, R., & Nkonga, B. (2014). Towards the direct numerical simulation of nucle-  
612 ate boiling flows. *International Journal of Multiphase Flow*, 66, 62–78.
- 613 Le Métayer, O., & Saurel, R. (2015). An alternative to cubic equations of state: The Noble-Abel—  
614 “stiffened gas” equation of state. *International Journal of Thermal Sciences* (submitted).
- 615 Le Métayer, O., Massoni, J., & Saurel, R. (2004). Elaboration des lois d’état d’un liquide et de sa  
616 vapeur pour les modèles d’écoulements diphasiques. *International Journal of Thermal Sciences*,  
617 430(3), 265–276.
- 618 Lund, H. (2012). A hierarchy of relaxation models for two-phase flow. *SIAM Journal on Applied  
619 Mathematics*, 720(6), 1713–1741.
- 620 Menikoff, R., & Plohr, B.J. (1989). The Riemann problem for fluid flow of real materials. *Reviews  
621 of Modern Physics*, 610(1), 75.
- 622 Murrone, A., & Guillard, H. (2005). A five equation reduced model for compressible two phase  
623 flow problems. *Journal of Computational Physics*, 2020(2), 664–698.
- 624 Saurel, R., Petitpas, F., Abgrall, R., et al. (2008). Modelling phase transition in metastable liquids:  
625 Application to cavitating and flashing flows. *Journal of Fluid Mechanics*, 6070(1), 313–350.
- 626 Simoes-Moreira, J. R., & Shepherd, J. E. (1999). Evaporation waves in superheated dodecane. *Jour-  
627 nal of Fluid Mechanics*, 382, 63–86.
- 628 Sinibaldi, E., Beux, F., & Salvetti, M. V. (2006). A numerical method for 3D barotropic flows in  
629 turbomachinery. *Flow, Turbulence and Combustion*, 760(4), 371–381.
- 630 Toro, E. F. (2009). *Riemann solvers and numerical methods for fluid dynamics: A practical intro-  
631 duction*. Springer Science & Business Media.
- 632 Toro, E. F., Spruce, M., & Speares, W. (1994). Restoration of the contact surface in the HLL-  
633 Riemann solver. *Shock Waves*, 40(1), 25–34.
- 634 Wood, A. B. (1930). *A textbook of sound*. London: G. Bell and Sons Ltd.

# Author Queries

Chapter 10

---

Query Refs.	Details Required	Author's response
	No queries.	

UNCORRECTED PROOF

# MARKED PROOF

## Please correct and return this set

Please use the proof correction marks shown below for all alterations and corrections. If you wish to return your proof by fax you should ensure that all amendments are written clearly in dark ink and are made well within the page margins.

<i>Instruction to printer</i>	<i>Textual mark</i>	<i>Marginal mark</i>
Leave unchanged	... under matter to remain	Ⓟ
Insert in text the matter indicated in the margin	∧	New matter followed by ∧ or ∧ <sup>Ⓢ</sup>
Delete	/ through single character, rule or underline or ┌───┐ through all characters to be deleted	Ⓞ or Ⓞ <sup>Ⓢ</sup>
Substitute character or substitute part of one or more word(s)	/ through letter or ┌───┐ through characters	new character / or new characters /
Change to italics	— under matter to be changed	↙
Change to capitals	≡ under matter to be changed	≡
Change to small capitals	≡ under matter to be changed	≡
Change to bold type	~ under matter to be changed	~
Change to bold italic	≈ under matter to be changed	≈
Change to lower case	Encircle matter to be changed	≡
Change italic to upright type	(As above)	⊕
Change bold to non-bold type	(As above)	⊖
Insert 'superior' character	/ through character or ∧ where required	Υ or Υ under character e.g. Υ or Υ
Insert 'inferior' character	(As above)	∧ over character e.g. ∧
Insert full stop	(As above)	⊙
Insert comma	(As above)	,
Insert single quotation marks	(As above)	ʹ or ʸ and/or ʹ or ʸ
Insert double quotation marks	(As above)	“ or ” and/or ” or ”
Insert hyphen	(As above)	⊞
Start new paragraph	┌	┌
No new paragraph	┐	┐
Transpose	└┐	└┐
Close up	linking ○ characters	Ⓞ
Insert or substitute space between characters or words	/ through character or ∧ where required	Υ
Reduce space between characters or words		↑